35th Annual International Conference of the IEEE EMBS
Osaka, Japan, 3 - 7 July, 2013

# Influence of Active Dendrites on Firing Patterns in a Retinal Ganglion Cell Model

Tianruo Guo, *Student Member, IEEE,* David Tsai, *Member, IEEE,* Sinisa Sovilj, *Member IEEE,* John W. Morley, Gregg J. Suaning, *Senior Member, IEEE*, Nigel H. Lovell, *Fellow, IEEE* and Socrates Dokos, *Member, IEEE*

***Abstract*—Active regional conductances and inhomogeneous distribution of membrane ionic channels in dendrites influence the integration of synaptic inputs in cortical neurons. How these properties shape the response properties of retinal ganglion cells (RGC) in the mammalian retina has remained largely unexplored. In this study, we used a morphologically-realistic RGC computational model to study how active dendritic properties contribute to neural behaviors. Our simulations suggest that the dendritic distribution of voltage-gated ionic channels strongly influences RGC firing patterns, indicating their important contribution to neuronal function.**

## I. Introduction

The presence of active membrane conductances in the dendrites of certain classes of retinal ganglion cell (RGC) dendrites are known to be important for visual information processing [1]. Along with dendritic morphology and synaptic connections, these active conductances can influence the synaptic inputs from bipolar cells and amacrine cells before these inputs arrive at the RGC soma [2-4]. The importance of active dendrites in shaping neuronal behaviors has been demonstrated in many classes of cortical neurons (for review, see [5]). Notwithstanding these findings, the significance of active dendrites in RGCs, and how they influence the integration of visual information in these sensory neurons, has remained largely unexplored. Computational studies can provide a mean of understanding how these RGC properties influence their behaviors.

As a step towards this goal, we have developed an active compartmental model with realistic RGC morphology to understand how active dendritic structures contribute to RGC behaviors. A conductance-based ionic model was used to reproduce RGC excitations in response to intracellular current stimuli. We included in the model representations of soma, axon initial segment (AIS), axon hillock (AH), axon and dendrites. We also varied the membrane ionic conductance in each neurite to reflect the properties of real neurons.

T. Guo, D.Tsai, S. Sovilj, G. J. Suaning, N. H. Lovell and S. Dokos are with the Graduate School of Biomedical Engineering, University of New South Wales, Sydney, 2052, Australia. David Tsai is also with Howard Hughes Medical Institute, Biological Sciences, Columbia University, New York, NY, USA and Bioelectronic Systems Lab, Electrical Engineering, Columbia University, New York, NY, USA. J. W. Morley is with School of Medicine, University of Western Sydney, Australia.

E-mail for correspondence: t.guo@unsw.edu.au.

Our results suggest a correlation between active dendritic structure and RGC firing patterns, revealing their significance in neuronal function.

## II. Methodology

The three dimensional, conductance-based RGC model used in this study was an extension of the Fohlmeister and Miller (1997) (FM) formulations [6]. Five voltage-gated ionic currents were present in the original work: fast sodium ($I_{Na}$), delayed-rectifying potassium ($I_K$), A-type potassium ($I_{KA}$), calcium ($I_{Ca}$), calcium-activated potassium ($I_{KCa}$). Here we added two additional currents, the hyperpolarization-activated current ($I_h$), and the low-voltage $Ca^{2+}$ current ($I_{CaT}$). A time-independent leakage current was also included in all compartments of the model RGC. The membrane ionic conductances varied in different regions of the RGC (Table I) to reflect the properties of real biological neurons. Furthermore, we optimized the conductances for all seven ionic currents, so that the firing patterns of the model neurons matched those of biological neurons during intracellular current injection. The membrane capacitance ($C_m$) was set to 1 $\mu F \cdot cm^{-2}$. Intracellular axial resistivity was set 110 $\Omega \cdot cm$. The simulation temperature was 35 °C. Full details of the RGC model and morphological reconstruction can be found in the accompanying papers [7, 8]. All simulations were performed and analyzed in NEURON 7.2 [9] and Matlab 2010 (Mathworks).

TABLE I.
Ionic Channel Distributions

| Channel | Regional Conductances ($mS/cm^2$) | | | | |
|---|---|---|---|---|---|
| | Soma | Axon | AIS | AH | Dendrites |
| $I_{Na}$ | 35.7 | 35.7 | 357 | 35.7 | 13.4 |
| $I_K$ | 13.1 | 13.1 | 13.1 | 13.1 | 8.73 |
| $I_{KA}$ | 39.4 | - | 39.4 | 39.4 | 26.3 |
| $I_{Ca}$ | 1.1 | - | 1.1 | 1.1 | 1.47 |
| $I_{KCa}$ | 0.047 | 0.047 | 0.047 | 0.047 | 7.22e-4 |
| $I_h$ | 0.19 | 0.19 | 0.19 | 0.19 | 0.19 |
| $I_{CaT}$ | 0.026 | 0.026 | 0.026 | 0.026 | 0.13 |
| $I_L$ | 0.012 | 0.012 | 0.012 | 0.012 | 0.012 |

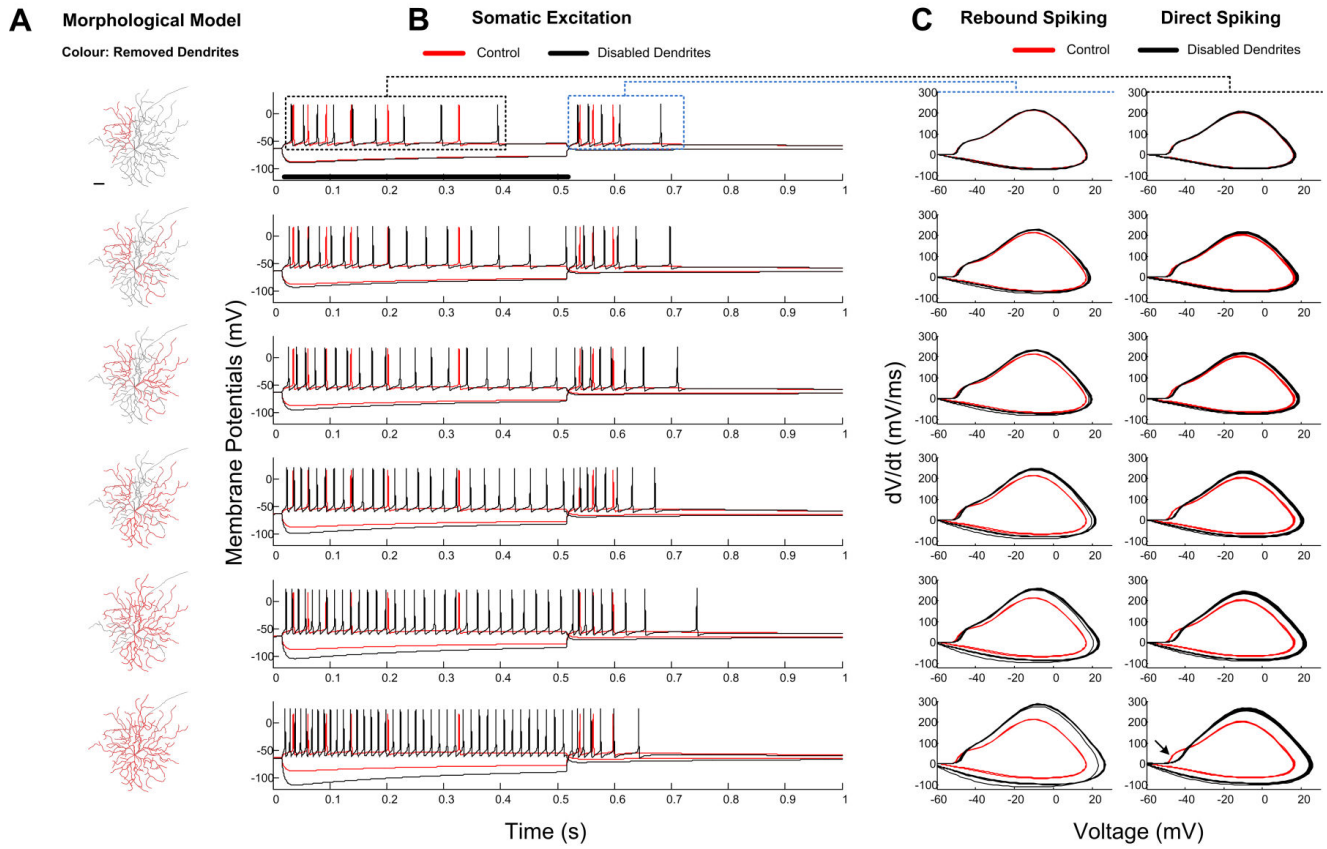


Fig. 1. Distinct firing patterns in the RGC model with identical biophysics but different active dendritic densities. A. RGC morphologies. Removed dendritic branches were labeled by corresponding colors. B. Membrane potentials in response to various somatic current injections before (red) and after (black) the removal of dendrites. Note the presence of both normal and rebound RGC spikes. External somatic current injection: 500 ms duration (horizontal bar) with amplitudes of 60 pA for depolarizing and -160 pA for hyperpolarizing injections. C. Phase plot (dV/dt versus V) of the somatic direct (right) and rebound (left) action potential triggered by depolarizing and hyperpolarizing simulation respectively. The elimination of initial segment soma dendritic break is indicated by the arrow.

## III. Results

### A. *Influence of active dendritic structure on RGC firing patterns*

We gradually removed the active dendritic tree by disconnecting dendritic branches from the full computer-reconstructed RGC geometry (Fig. 1A), and then simulated somatic membrane potentials in response to both depolarizing and hyperpolarizing somatic current injections. Each model was run for 500 ms before stimulation onset to reach steady state. The simulation results indicated progressively increasing spiking frequency and a reduction in first spike latency (FSL) with reduced dendritic branching (Fig. 1B). In addition, both direct and rebound AP waveforms (Fig. 1C), as shown by the rate of voltage change (phase plot), were affected. These included increasing rates of rising/falling phases, increases in AP peak overshoot, as well as decreasing interspike interval (ISI). In particular, the initial segment-soma dendritic (IS-SD) break in the phase plot (labeled by the arrow in Fig. 1C) was progressively eliminated as more active dendritic branches were removed. To quantify the change of the phase plot (see Fig. 2), a custom

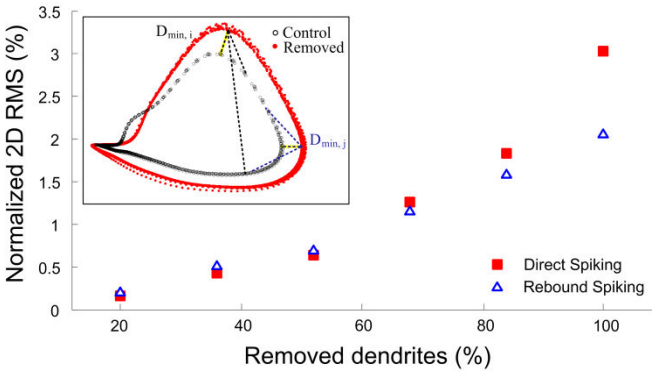


Fig. 2. Quantitative calculation of AP shape change. 2D normalized RMS value for both direct and rebound AP was increased when dendrites were progressively removed. Inset: The minimal 2D distance between two normalized phase plots was measured at each data point.

normalized two-dimensional RMS was defined by $\mathrm{RMS}_{2D,norm} = \sqrt{\sum(D_{min,j})^2/(N-1)}$, where $D_{min,j}$ represents the minimal normalized distance ($D_j$) from one phase plot to another at the $j$th point, $N$ is the number of data points in one phase plot, and $D_j = \sqrt{(V_{1,j}-V_{2,j})^2 + (dV_{1,j}/dt - dV_{2,j}/dt)^2}$, where $V_1$ and $V_2$ are normalized voltage values at the $j$th data point (see Fig. 2).

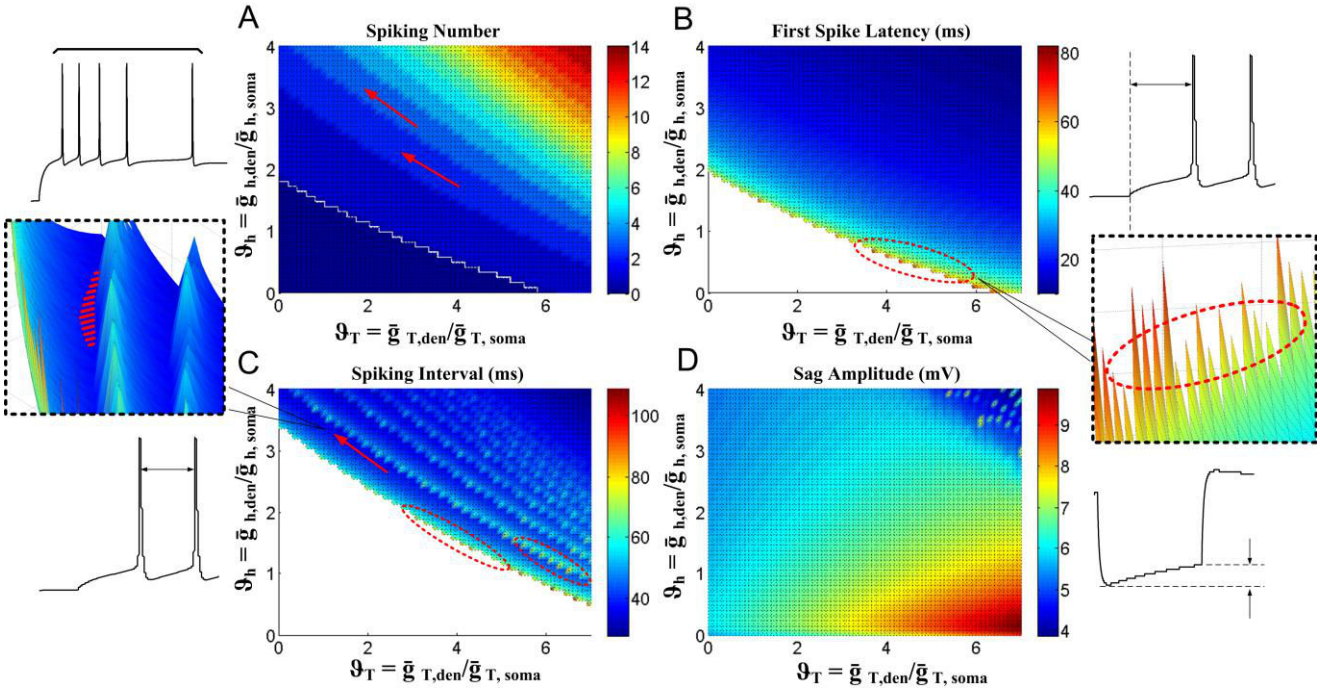


Fig. 3. Firing pattern sensitivity to somato-dendritic distribution of $I_h$ and $I_{CaT}$ ($\vartheta_h = \bar{g}_{h,den}/\bar{g}_{h,soma}$ and $\vartheta_T = \bar{g}_{T,den}/\bar{g}_{T,soma}$). A. Rebound Spiking number as a function of $\vartheta_h$ and $\vartheta_T$. B. First spike latency (measured as the time difference between the stimulation termination and half-maximum amplitude of the first dendritic AP) as a function of $\vartheta_h$ and $\vartheta_T$. C. Averaged spiking interval as a function of $\vartheta_h$ and $\vartheta_T$. D. Sag amplitude (measured as peak-to-steady state potential difference) during hyperpolarizing stimulation as a function of $\vartheta_h$ and $\vartheta_T$. The empty space (white) in B and C represent regions without an AP.

### B. *Influence of dendritic ionic channel distributions*

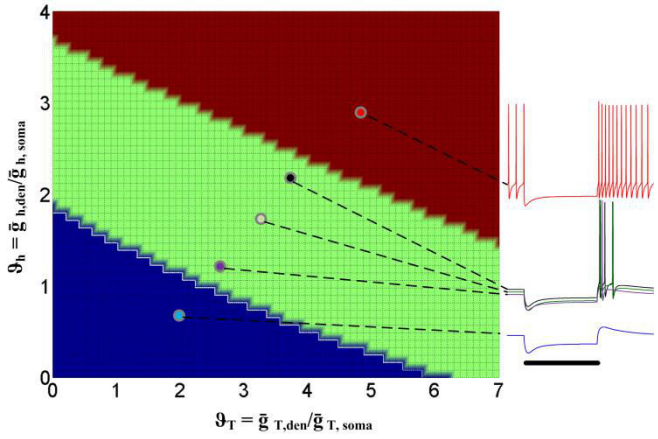


Fig. 4. Dependency of activity state on somato-dendritic distribution of $I_h$ and $I_{CaT}$. Blue: Passive cell. Green: Rebound cell. Red: Spontaneous cell. Horizontal bar: hyperpolarizing stimulation time (500 ms duration, -120 pA amplitude). Examples of typical RGC responses in each state and their parameter locations are illustrated at right.

To test the sensitivity of RGC firing patterns to dendritic ionic current distribution, we set the somato-dendritic channel distribution ratio of $I_h$ and $I_{CaT}$ (defined by $\vartheta_j = \bar{g}_{j,den}/\bar{g}_{j,soma}$,) as indicators of RGC rebound firing properties, where $\bar{g}_{j,den}$ and $\bar{g}_{j,soma}$ represent the maximum membrane conductance of the corresponding ionic current in the soma and dendrites respectively. We chose these two currents because of their absence in the original FM model and importantly, their contribution to cell responses due to hyperpolarizing stimuli. The two ratios $\bar{g}_{h,den}/\bar{g}_{h,soma}$ and $\bar{g}_{T,den}/\bar{g}_{T,soma}$, were varied over the ranges 0~4 and 0~7, respectively. We calculated four response properties in the model neurons: rebound spiking number; FSL; ISI and depolarizing sag amplitude (Fig.3). Analysis was undertaken at the soma to characterize the RGC activities in response to hyperpolarizing somatic injection (500 ms duration, 160 pA amplitude).

The results suggested correlations between certain spiking properties. Rebound spiking number (Fig. 3A) and averaged spiking interval (Fig. 3C) showed a close match of their 'waves' in parameter space. Moreover, we found sensitive (as indicated by red ovals in Fig. 3B, C) and insensitive parameter regions (red arrows in Fig. 3A, C), where the model exhibited dramatic and stable firing patterns respectively in response to parameter tweaking. Note that individual membrane response property may not provide enough information on the global structure of RGC models. For example, ISIs (Fig. 3C) were almost absent in the region of $\vartheta_h \in (0, 1.5)$ and $\vartheta_T \in (0, 4.5)$, where the sag amplitude map (Fig. 3D) became more useful, since this quantity was present over the whole parameter space investigated.

The sensitivity of RGC activity state to somato-dendritic channel distribution ratio is shown in Fig. 4. RGCs are classified as passive (no rebound spiking after termination of hyperpolarizing injection), rebound or spontaneous cell (excited before stimulus was injected). The activity states also showed strong correlations to firing properties in Fig. 3. We found that the sensitive space of firing properties such as FSL

and ISI, are typically near the boundary between different activity states.

## IV. Discussion and Conclusion

To isolate the contribution of active dendrites, the set of morphological RGC models shared identical ionic channel kinetics and distribution, differing only in their active dendritic structures. Marked increase in the rising and falling phase of the phase plot can be explained by the presence of higher somatic $Na^+$ and $K^+$ currents with less active dendrites (Fig. 1C). The existence of IS-SD break, explained by the presence of high $Na^+$ channel density in the AIS, corresponds to spike initiation. The reduction of IS-SD break with less active dendrites revealed the moving location of AP initiation [10]. Considering the dendrites have larger overall membrane surface area and lower active membrane conductances compared with the soma, the fast ionic currents (e.g. $Na^+$) can be filtered, revealing the temporal low-pass filtering properties of the dendritic structure. The progressively increased spiking frequency with less branching (Fig. 1B) strongly supports this point.

Limited experimental information on RGC ionic channel distribution makes model parameter setting a difficult task. However, sensitivity analysis based on channel distributions can offer information on how neurons regulate their channels to maintain the desired excitation. Rather than analyzing their distributions in a given region, we considered the distribution ratios to provide more information about the interaction between soma and active dendrites. The firing pattern sensitivity to dendritic $I_h$ and $I_{CaT}$ (Fig. 3) provided a continuous spectrum of RGC firing properties in response to hyperpolarizing input. Recent experimental evidence in RGCs have suggested the presence of higher $I_{CaT}$ density in dendrites [11]. Despite the limited experimental information on $I_h$ distribution in RGCs, this current was found to have higher density (sixfold to somatic density) in CA1 pyramidal neuron dendrites [12]. We noted that RGC activities are a result of the interaction between all its membrane conductances, and not only a result of $I_h$ and $I_{CaT}$. However, these two currents were both absent in the original FM model. Furthermore, both channels are responsible for neuron activities in response to hyperpolarizing stimuli. Thus, at the very least, our sensitivity analysis provides information on how the presence of these new ionic currents contributes to cell behaviours. In future studies, we intend to extend our method to include more conductances to explore the higher dimensional RGC parameter space.

Three dimensional plots of model behaviors in response to various channel distributions can also provide a clear global map of activity states of the RGC. Nearly identical activities can be reproduced by different combinations of dendritic $I_h$ and $I_{CaT}$ conductances. On the other hand, the model behaviors can be highly sensitive to parameter tweaking, especially in the region near the boundary between different activity states. Interestingly, some experimental evidence has suggested the presence of large channel density variations in the same functionally-identified neuron types [13], while other studies have found that neuron activities were very sensitive despite small variations in channel expression [14].

In summary, our results suggest that physical properties of the dendritic tree provide the framework for dendritic signal processing while dendritic active conductances can further 'tweak' spiking properties through the interaction between dendrites and the soma-axon compartment. This modeling approach provides a promising tool for studying dendritic mechanisms of RGCs, assisting experimental studies in dendritic patch-clamp recording, fluorescent imaging and immunocytochemical channel localization techniques.


## Acknowledgment

This research was supported by the Australia Research Council (ARC) through a Special Research Initiative (SRI) in Bionic Vision Science and technology grant to Bionic Vision Australia (BVA).


## References


[1] N. Oesch, T. Euler, and W. R. Taylor, "Direction-selective dendritic action potentials in rabbit retina," *Neuron,* vol. 47, pp. 739-750, 2005.

[2] T. J. Velte and R. H. Masland, "Action potentials in the dendrites of retinal ganglion cells," *J Neurophysiol,* vol. 81, pp. 1412-1417, 1999.

[3] D. J. Margolis, A. J. Gartland, T. Euler, and P. B. Detwiler, "Dendritic calcium signaling in ON and OFF mouse retinal ganglion cells," *J Neurosci,* vol. 30, pp. 7127-7138, 2010.

[4] M. J. Schachter, N. Oesch, R. G. Smith, and W. R. Taylor, "Dendritic spikes amplify the synaptic signal to enhance detection of motion in a simulation of the direction-selective ganglion cell," *Plos Comput Biol,* vol. 6, 2010.

[5] G. Stuart, N. Spruston, B. Sakmann, and M. Hausser, "Action potential initiation and backpropagation in neurons of the mammalian CNS," *Trends Neurosci,* vol. 20, pp. 125-131, 1997.

[6] J. F. Fohlmeister and R. F. Miller, "Impulse encoding mechanisms of ganglion cells in the tiger salamander retina," *J Neurophysiol,* vol. 78, pp. 1935-1947, 1997.

[7] T. Guo, D. Tsai, J. W. Morley, G. J. Suaning, N. H. Lovell, and S. Dokos, "Cell-specific modeling of retinal ganglion cell electrical activity," in *Engineering in Medicine and Biology Society (EMBC), 2013 Annual International Conference of the IEEE*, accepted.

[8] T. Guo, D. Tsai, J. W. Morley, G. J. Suaning, N. H. Lovell, and S. Dokos, "Influence of Cell Morphology in a Computational Model of ON and OFF Retinal Ganglion Cells," in *Engineering in Medicine and Biology Society (EMBC), 2013 Annual International Conference of the IEEE*, accepted.

[9] M. L. Hines and N. T. Carnevale, "The NEURON simulation environment," *Neural Computation,* vol. 9, pp. 1179-1209, 1997.

[10] B. W. Sheasby and J. F. Fohlmeister, "Impulse encoding across the dendritic morphologies of retinal ganglion cells," *J Neurophysiol,* vol. 81, pp. 1685-1698, 1999.

[11] R. F. Miller, K. Stenback, D. Henderson, and M. Sikora, "How voltage-gated ion channels alter the functional properties of ganglion and amacrine cell dendrites," *Arch Ital Biol,* vol. 140, pp. 347-359, 2002.

[12] J. C. Magee, "Dendritic hyperpolarization-activated currents modify the integrative properties of hippocampal CA1 pyramidal neurons," *J Neurosci,* vol. 18, pp. 7613-7624, 1998.

[13] J. Golowasch, L. F. Abbott, and E. Marder, "Activity-dependent regulation of potassium currents in an identified neuron of the stomatogastric ganglion of the crab Cancer borealis," *J Neurosci,* vol. 19, p. RC33, 1999.

[14] M. S. Goldman, J. Golowasch, E. Marder, and L. F. Abbott, "Global structure, robustness, and modulation of neuronal models," *J Neurosci,* vol. 21, pp. 5229-5238, 2001.